



# Separation of Lithium Ions from Aqueous Solutions Using Membrane Aided Separation Techniques

T. Aswani<sup>1</sup>, P. Uma Maheswari<sup>2</sup>, Sugali Chandra Sekar<sup>3</sup>, M. Kalyan Kumar<sup>4</sup>.

<sup>1,2,4</sup>Department of Chemical Engineering, JNTUA College of Engineering Ananthapuramu,

<sup>1,2,4</sup>Affiliated to JNTU Anantapur, Ananthapuramu, Andhra Pradesh, 515002, India.

<sup>3</sup>Membrane Separation Laboratory, CE & PT Division, CSIR- Indian Institute of Chemical Technology, Tarnaka, Hyderabad, Telangana, 500007, India.

(Received: 07 January 2024

Revised: 12 February 2024

Accepted: 06 March 2024)

KEYWORDS	ABSTRACT:
Nanofiltration membrane, Hydrophilized polyamide membrane, Iron nanoparticles, Polyacrylonitrile (PAN), Sodium dodecyl sulfate (SDS), Micelle, Lithium concentration, Rejection.	<p>Lithium production is crucial for sustainable development. Lithium ions have been used in battery technology, ceramics, and polymer production. Membrane processes like reverse osmosis and electrodialysis are trending for lithium recovery. However, high energy consumption is still a challenging problem in lithium recovery. To reduce the cost and membrane fouling, the present study focused on the development of PAN-Fe<sub>2</sub>O<sub>3</sub> membranes. The chemical structure, surface morphology, and chemical compounds of a commercial HPA50 membrane and fabricated PAN-Fe<sub>2</sub>O<sub>3</sub> membranes were characterized by XRD, SEM and FTIR respectively. Lithium ions are separated by micellar enhanced ultrafiltration with sodium dodecyl sulfate (SDS) surfactant employing commercial hydrophilized polyamide membrane and PAN membranes blended with varying concentrations of iron nanoparticles (0.005%, 0.01%, and 0.1%). Experiments were conducted by varying the feed concentration and operating pressure. The chemical structure was confirmed by XRD analysis, which showed peaks at 20°, 23°, and 25° for HPA50 membrane at 18°, 23°, and 26° for PAN-Fe<sub>2</sub>O<sub>3</sub> membranes. FTIR analysis identified amide functional groups for the HPA50 membrane and nitrile groups for PAN-Fe<sub>2</sub>O<sub>3</sub> membranes. Additionally, SEM analysis confirmed the uniform and stable attachment of particles on the surface of both HPA50 and PAN-Fe<sub>2</sub>O<sub>3</sub> membranes. HPA50 membrane, utilized for lithium-ion separation, exhibited rejection rates of 40%, 85%, and 83.9% at operating pressures of 0 bar, 1 bar, and 2 bar, respectively, when employed with a LiCl aqueous feed solution. Subsequently, experiments conducted with LiCl and SDS surfactant yielded higher rejection rates of 89.40%, 93%, and 83.90%. There is no rejection observed in PAN-Fe<sub>2</sub>O<sub>3</sub> membranes due to large pore sizes. The HPA50 membrane rejection rates indicate that the separation of Li<sup>+</sup> ions from pure aqueous solutions is more difficult than the separation from divalent ions in mixed solutions. ICP-MS of reject samples showed a higher peak area, indicating separation. Addition of SDS to the feed with HPA50 membrane enhanced lithium ion rejection. PAN-Fe<sub>2</sub>O<sub>3</sub> membranes are found to be ineffective due to large pore sizes for concentrating lithium ions.</p>

## 1. Introduction

Lithium, found in Group I of the periodic table after hydrogen, has an atomic number of 3 and an atomic weight of 6.9 g/mol. As a highly reactive metal belonging to the alkali metal group, it has a density 0.534 g/cm<sup>3</sup>. Lithium is distinctive for being the lightest solid element and one of the least dense metals. It is commonly kept in mineral oil (Fig. 1) because it reacts

with the moisture in the air. Lithium and its compounds are industrially significant, sourced mainly from brine deposits and pegmatite ores such as spodumene, lepidolite, and amblygonite. These ores typically contain lithium oxide (Li<sub>2</sub>O) concentrations between 4 and 8.5 percent. Lithium is present in the Earth's crust at approximately 0.002 percent. The primary commercial form is lithium carbonate (Li<sub>2</sub>CO<sub>3</sub>), derived from



pegmatite ores and brine deposits. Lithium chloride (LiCl) is produced from lithium carbonate, used in electrolysis to obtain lithium metal. During electrolysis, lithium metal is separated from mixtures containing heavy metal ions such as  $Mg^{+2}$ ,  $Cd^{+2}$ ,  $Mn^{+2}$ , and  $K^{+}$ . Lithium exhibits similarities to elements in the alkaline earth group, particularly magnesium, sharing similar atomic and ionic radii.



**Figure 1.** Lithium in mineral oil

Lithium's primary and widely recognized application lies in rechargeable batteries, particularly lithium-ion batteries, introduced in the 1970s. These batteries have revolutionized portable electronics and have become the predominant power source for devices like smartphones, laptops, electric vehicles, and various other portable gadgets. This dominance stems from lithium's efficiency in storing and releasing electrical energy, crucial for advancing modern technology.

The demand for lithium has surged further in recent years due to the growth of the electric vehicle industry and increasing interest in renewable energy sources. Its exceptional properties have led to applications in various fields including technology, ceramic glasses, lubricating greases, air treatment, pharmaceuticals, and polymer production. Lithium's significance is pivotal in shaping the modern world and remains essential for future technological advancements.

In 2020, lithium production was dominated by Australia (52%), followed by Chile (25%), China (13%), Argentina (6%), the US (1%), and Brazil (1%). The demand for lithium is estimated to reach 1.5 million tons of lithium carbonate equivalent by 2025 and exceed 3 million tons by 2030. Lithium reserves in India have accelerated the growth of the electric vehicle industry. Out of total reserves of 104 million tons, India ranks 7<sup>th</sup> largest lithium resource globally with 5.9 million tons of reserves along countries like Bolivia, Argentina, US,

Chile, Australia, China, India, Germany, DR Congo, Canada and other countries (Fig. 2).

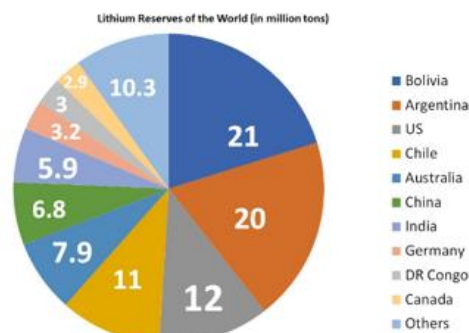


**Figure 2.** Lithium Reserves of the world (in million tons)

### 1.1 Lithium sources

The main sources of lithium include pegmatite ore, brine, and clay deposits (Fig. 3). Pegmatite ores, commonly mined using traditional hard rock mining methods, yield lithium, with spodumene being the most frequently extracted mineral.

Lithium rich brines, located in underground reservoirs often found in salt, are concentrated through evaporation in large ponds, leading to the extraction of lithium-rich salts. Furthermore, lithium can be extracted from clay minerals like hectorite and montmorillonite, typically found in sedimentary formations. Various techniques are utilized to process these deposits and extract lithium [1].

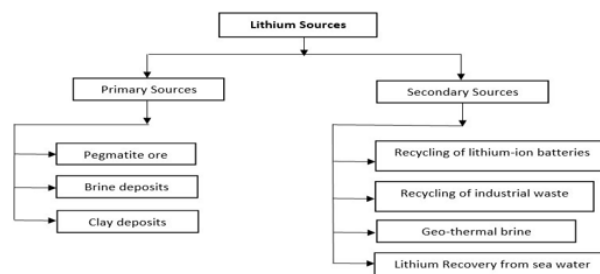


**Figure 3.** Classification of lithium sources

Secondary sources of lithium offer potential for mitigating the environmental impact of extraction and enhancing the sustainability of lithium-based products. These sources involve extracting lithium from recycled materials rather than directly from primary deposits. Lithium-ion batteries, widely used in electronic devices, electric vehicles, and energy storage systems, contain significant amounts of lithium (Fig. 3). Recycling these



batteries allows for lithium recovery, which can be reused in new battery production. Additionally, certain industrial processes, such as ceramics, glass, and aluminium production, generate waste streams containing lithium. Recovering lithium from these streams using specialized methods provides another secondary source. Furthermore, some geothermal energy production sites yield brines with high lithium concentrations, serving as additional secondary sources.

### 1.2 Methods used for lithium ion separation

Membrane technology is promising over conventional methods such as adsorption, distillation, etc. due to its low cost, less footprint, less chemical usage, and eco-friendly characteristics. Several membrane processes like reverse osmosis, and electro dialysis methods are in trend for lithium recovery due to their high rejection capacity and easy operation. However high energy consumption is still a challenging problem in lithium recovery. Methods are classified into two traditional and conventional methods [1]. Traditional methods include solvent extraction, chemical precipitation, and solar evaporation. When  $\text{LiCO}_3$  is combined with unwanted salts such as  $\text{NaCl}$ ,  $\text{Mg(OH)}_2$ , and  $\text{K}^+$ , solar evaporation takes longer to extract lithium from the mixed divalent ions ( $\text{Mg}^{+2}$ ,  $\text{Ca}^{+2}$ , &  $\text{Na}^{+2}$ ),  $\text{MgCO}_3$  also requires additional purification. Conventional methods used for lithium recovery are liquid-liquid extraction, ion-imprinted mechanism, ion-sieve mechanism, membrane distillation crystallization (MDC), and electro dialysis (ED).

The liquid-phase polymer-based retention technique (LPR), micellar enhanced ultrafiltration (MEUF), and polymer-enhanced ultrafiltration (PEUF) are different from conventional separation methods for the separation of salts or solutes. These processes require low pressure conditions for interaction between metal ions and surfactants, leading to the formation of macromolecular aggregates that can be trapped by the membrane [2,3, & 4].

## 2. Objective

The aim of the present study is to prepare PAN membranes blended with different concentrations of iron nanoparticles for the separation of lithium ions from aqueous solutions by micellar-enhanced

ultrafiltration (MEUF) technique using sodium dodecyl sulfate (SDS) surfactant.

The study also focuses on the impact of process variables, such as upstream pressure and initial lithium concentration on membrane flux and rejection rate of lithium ions.

## 3. Materials and methods

### 3.1 Materials and Chemicals

All reagents were used without purification (Table 1). Deionized water was produced for sample preparation using a laboratory reverse osmosis (RO) membrane-cascaded system. Borosil Limited, India, made glassware including conical flasks, petri dishes, beakers, and measuring cylinders were used. Digital weighing equipment and a magnetic stirrer were made by Remi, India.

Table 1. List of chemicals

S. No.	Chemical name	Supplier
1	Lithium Chloride (LiCl)	Sigma-Aldrich (USA)
2	Sodium dodecyl sulfate (SDS)	Sigma-Aldrich (USA)
3	Polyacrylonitrile (PAN)	Solvay Specialties India Pvt. Ltd., Gujarat, India.
4	Dimethylformamide (DMF)	Avra Laboratories in Hyderabad
5	Iron nanoparticles ( $\text{Fe}_3\text{O}_4$ )	Finer chemicals, Gujarat, India.

### 3.2 Commercial HPA50 membrane (M1)

A spiral wound hydrophilized polyamide membrane (HPA50) and polyester non-woven fabric support made by Permionics Membrane Pvt. Ltd., Vadodara, India are used. Commercial HPA50 membrane is a high flux nanofiltration membrane supported by PES substrate modified by monomers [5] that include 1% piperazine in an aqueous solution to form ultra-thin selective layer of piperazine-amine by interfacial polymerization (IP) and trimesoyl chloride (TMC) in hexane solution to obtain a thermally crosslinked NF membrane (Fig. 4).



Figure 4. Commercial HPA50 membrane



### 3.3 Preparation of PAN-Fe<sub>2</sub>O<sub>3</sub> membranes

The phase inversion approach was used to produce an iron oxide nanocomposite ultrafiltration membrane. Initially, 0.005 wt% iron oxide nanoparticles were added to 95.33 ml DMF solvent and sonicated for 30 minutes to ensure homogenous dispersion of nanoparticles in solution. Following this, polyacrylonitrile (PAN) a synthetic polymer of 10 wt% dissolved in DMF solvent while continuously stirring at 250 rpm for 24 hours (Fig. 5).

After forming a uniform honey-like viscous solution, it was placed in a desiccator to eliminate air bubbles. The produced polymeric solution was cast on a polyester fabric support using a casting machine with a doctor's blade to maintain a thickness of 120 μm. The casted polymeric substrate blended with iron nanoparticles was submerged in a non-solvent bath (deionized water) immediately to initiate phase inversion. Solvent molecules on the polymeric substrate were replaced with water molecules by forming ultra-sized pores. Further, the polymeric substrate was kept in the water bath until used for further experiments. The membrane obtained is denoted as M2.

Similarly, PAN membranes M3 and M4 were synthesized, by maintaining the same concentration of PAN polymer, DMF solvent, speed of stirring, sonication time, and thickness of the membrane with 0.01 wt% and 0.1% concentrations of iron nanoparticles respectively (Table 2).

### 3.4 Membrane Characterization

Membrane characterization involves utilizing

technique such as scanning electron microscopy

**Table 2.** Composition of the prepared PAN-Fe<sub>2</sub>O<sub>3</sub> membranes

S. No.	Membrane	PAN (wt%)	Fe <sub>2</sub> O <sub>3</sub> (wt%)	DMF (ml)
1	M2	10.005	0.005	95.333
2	M3	10.01	0.01	95.328
3	M4	10.1	0.1	95.233

(SEM), X-ray Diffraction (XRD), and Fourier-transform infrared spectroscopy (FTIR) to assess the physical, chemical, and structural properties of membranes used for applications such as filtration, separation, and purification.

#### 3.4.1 Chemical structure

Commercial HPA50 and fabricated composite PAN-Fe<sub>2</sub>O<sub>3</sub> membranes were characterized using X-ray diffractometer (Siemens D5000 model) to analyze their crystalline nature. X-ray diffraction with a CuK-alpha source generating wavelengths of 1.5 Å° was employed for this purpose.

#### 3.4.2 Identification of functional groups

FTIR spectroscopy, performed using a Nicolet740 Perkin-Elmer-283B FTIR Spectrometer, determined the spectra of nanoparticles and their composites, confirming existing functional groups in the polymer matrix and any additives or fillers present in the composite membrane.

#### 3.4.3 Morphology

Morphological studies of the synthesized membranes were conducted using a JSM 5410 digital scanning

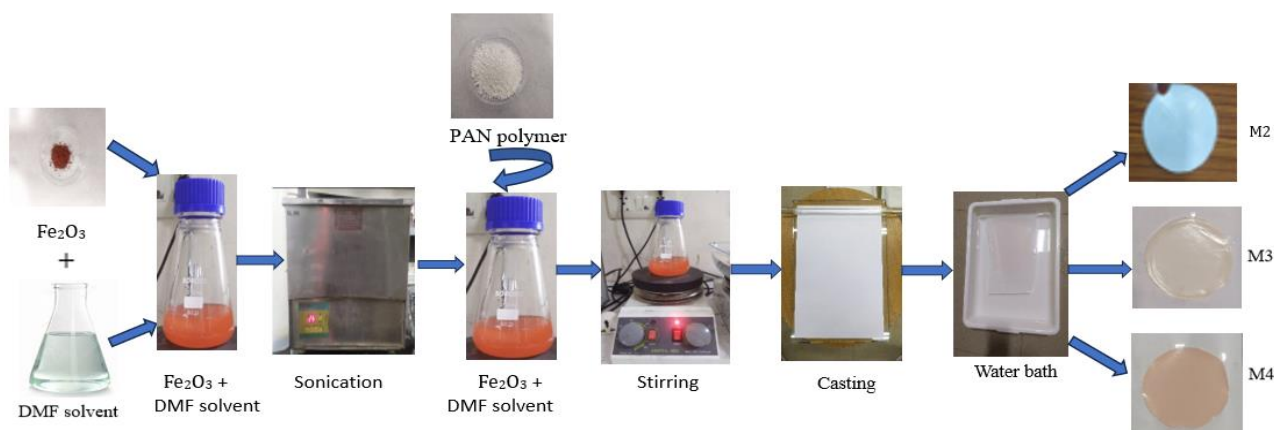


**Figure 5.** Synthesis of PAN- Fe<sub>2</sub>O<sub>3</sub> membranes



electron microscope from Japan. Samples were prepared under liquid nitrogen conditions, fractured, and coated with a thin layer of gold before examination via SEM to reveal surface and cross-sectional views at various magnifications. The size of nanoparticles present in the PAN-Fe<sub>2</sub>O<sub>3</sub> is determined by the Image-J software.

### 3.5 Membrane performance tests

Pure water flux serves as a crucial parameter in evaluating membrane performance across various applications like water treatment, desalination, and wastewater reuse. It is calculated by measuring the volume of permeate collected over time under conditions of constant pressure. Maintaining a steady driving force, such as pressure and temperature, is essential to ensure accurate flux measurements.

Pure water flux can be calculated by

$$J_w = \frac{\Delta V}{\Delta t \times A} \quad \text{----- (1)}$$

where  $J_w$  (L.m<sup>-2</sup>.h<sup>-1</sup>) is the pure water flux,  $\Delta V$  (L) is volume of permeate collected,  $A$  (m<sup>2</sup>) is the surface area of the membrane, and  $\Delta t$  (h) is time intervals of the samples for every 50 ml.

### 3.6 Separation performance tests

Time vs. flux studies, are highly important in separation science, particularly in isolating metal ions and other compounds from complex mixtures. Experimental studies involve adjusting factors like solvent composition, pH, temperature, and flow rate to optimize conditions for enhanced separation efficiency while minimizing analysis duration.

The rejection of Li<sup>+</sup> ions is calculated by

$$R (\%) = \left( \frac{C_f - C_p}{C_f} \right) \times 100 \quad \text{----- (2)}$$

where  $R$  (%) is the removal percentage of lithium ions,  $C_f$  is the concentration of feed in TDS,  $C_p$  is the concentration of permeate in TDS.

### 3.7 Experimental set-up of HPA50 Membrane

The system consists of a 0.3 m<sup>2</sup> area of spiral wound configuration of HPA50 membrane, fixed in a tubular

housing (Fig. 6). The housing of the membrane module has one feed inlet and two outlets, one for permeate and the other one for reject. A diaphragm pump is used for feed flow from the feed tank to the membrane module. A pressure gauge and a control valve to regulate flow are provided in the reject line.

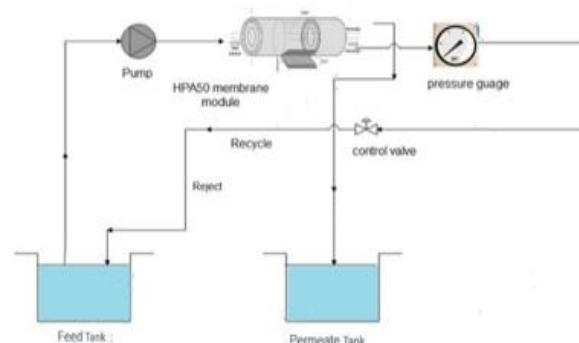


**Figure 6.** Point flow diagram for a spiral membrane

### 3.7.1 Lithium ion separation using HPA50 membrane with and without surfactant

A 0.06 wt % LiCl aqueous solution was fed to the HPA50 membrane at operational gauge pressures of 0.5 bar, 1 bar, and 2 bar. Permeate samples were drawn at regular intervals to assess volumetric flow, and samples (feed, permeate, and reject) were stored at ambient temperatures for analysis of pH, conductivity, and TDS parameters.

- Similar studies were conducted by adding 0.3 wt% SDS surfactant to the LiCl aqueous solution. At 0.3 wt% concentrations, surfactant micelles start to form with lithium ions [6]. The trials were carried out using the MEUF technique to get the resultant parameters.
- An aqueous solution was prepared with MgCl<sub>2</sub> and LiCl in mass ratio Mg<sup>2+</sup>/Li<sup>+</sup>=2.4, and passed through an HPA50 membrane at a gauge pressure of 1 bar. Permeate samples were taken at regular intervals to determine flux. Feed, permeate, and reject samples are stored at ambient temperatures for pH, conductivity, and TDS analysis.

### 3.8 Lab-scale experimental setup of cross-flow filtration

A laboratory-scale cross-flow filtration experimental setup was used for testing all synthesized membranes



(Fig. 7). The setup consists of a pump, membrane module, pressure gauge, and valves. A pump is used to pass the feed into a membrane module to produce retentate and permeate.

The membrane module, consisting of a polymeric membrane helps to retain the high molecular weights on the reject side and the low molecular weight particles on the permeate side. A pressure gauge serves to indicate the pressures which are used for the feed and permeate flows. The effective area of the membrane is 0.011 m<sup>2</sup>.

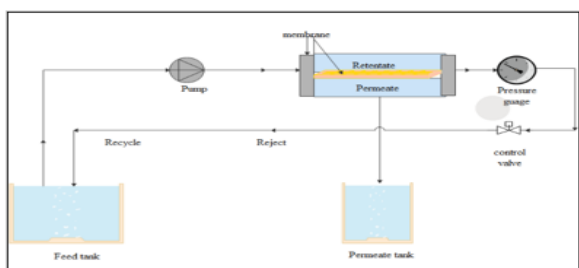


**Figure 7.** Point flow diagram for a cross-flow filtration

### 3.8.1 Lithium ion separation using PAN-Fe<sub>2</sub>O<sub>3</sub> membranes

A 0.06 wt % LiCl aqueous solution was fed over a flat sheet membrane at operational gauge pressures of 0.5 bar. Permeate samples were taken at regular intervals to assess volumetric flow. Samples of feed, permeate, and reject were held at ambient temperatures for pH, conductivity, and TDS analysis. Similar experiments were carried out for M3 and M4 membranes.

## 4. Results and discussion

### 4.1 Chemical structure by XRD

#### 4.1.1 HPA50 membrane

The thin film of HPA50 membrane (M1) was submitted to XRD for investigation of the crystalline structure and phase composition. The sharp peaks of the XR diffractogram represent that the particles are in crystalline nature (Fig. 8). The sharp peaks of the XR diffractogram at diffraction angles 20°, 23°, and 25°, with intensities 1380, 1150, and 1480 indicates amide layer including piperazine, TMC, and PVA randomly arranged on the surface of the PES substrate [13].

#### 4.1.2 PAN-Fe<sub>2</sub>O<sub>3</sub> membranes (M2, M3 & M4)

The XR diffractograms of membranes M2, M3, and M4 (Fig. 9, 10, & 11) display sharp peaks at 18°, 23°, and 26°. These peaks correspond to intensities of 1520, 1331, and 1646 for M2, 1520, 1305, and 1650 for M3, and 1644, 1400, and 1793 for M4 respectively. These consistent peaks suggest the presence of PAN-Fe<sub>2</sub>O<sub>3</sub> compounds in the thin film samples of these membranes [7 & 8].

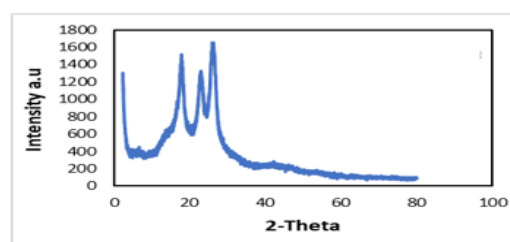


**Figure 9.** XRD of M2 membrane

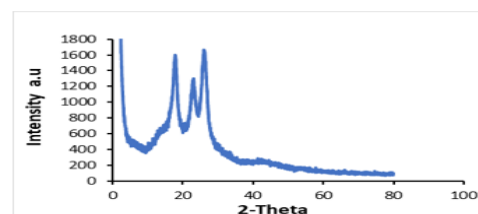


**Figure 10.** XRD of M3 membrane

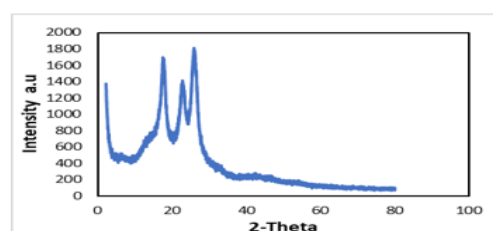


**Figure 11.** XRD of M4 membrane

The sharp peaks of XR diffractograms of membranes M2, M3, and M4 indicated that the particles are crystalline nature and the intensities of peaks are directly related to iron nanoparticle concentration [7 & 8].

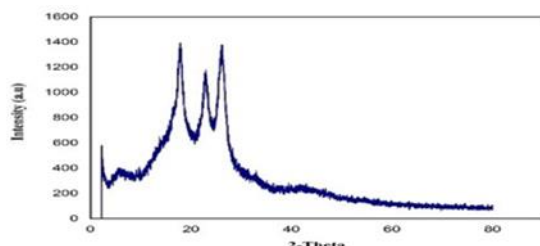


Figure 8. XRD of M1 membrane

#### 4.2 Identification of functional groups by FTIR

##### 4.2.1 HPA50 membrane (M1)

The Hydrophilized Polyamide Membrane (M1) is a composite NF membrane formed by an amide layer consisting of piperazine, TMC, and polyvinyl alcohol [13]. FTIR spectrum for membrane M1 was captured within the range of 0–4000  $\text{cm}^{-1}$  (Fig. 12).

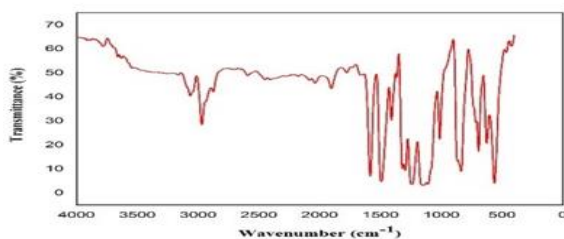


Figure 12. FTIR of M1 membrane

The FTIR analysis identified amines and methyl groups at particular wave numbers for M1 membrane (Table 3).

Table 3. FTIR analysis for HPA50 membrane (M1)

S. No.	Wave number ( $\text{cm}^{-1}$ )	Functional Group	Compound class	Comments
1	3000	N-H stretching	Amines	Intramolecular bond
2	1450	C-H bending	Alkane	methyl
3	1390	C-H bending	Alkane	dimethyl
4	1372	O-H bending	Alcohol	-
5	1225	S=O stretching	Sulfate	-

##### 4.2.2 PAN- $\text{Fe}_2\text{O}_3$ membranes (M2, M3, & M4)

The FTIR spectrum was recorded for the PAN membrane blended with iron nanoparticles in the range 0-3500  $\text{cm}^{-1}$  (Figs. 13, 14 & 15). The absorption bands at wavenumbers 2240, 2932, 1450 represent  $\text{-C}\equiv\text{N}$  stretching vibration of nitriles, C-H stretching and bending of methyl groups respectively (Fig. 13). Similar

absorption bands were observed for M3 and M4 membranes (Figs. 14 & 15).

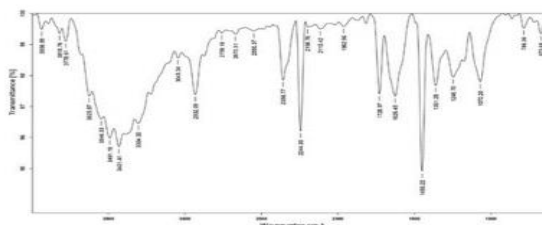


Figure 13. FTIR of M2 membrane

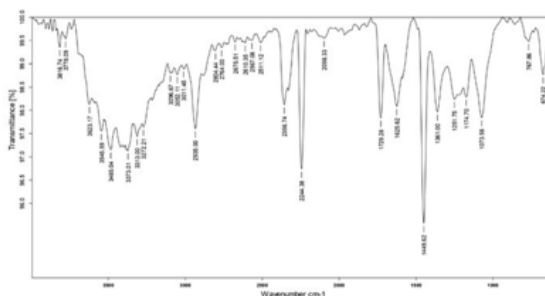


Figure 14. FTIR of M3 membrane

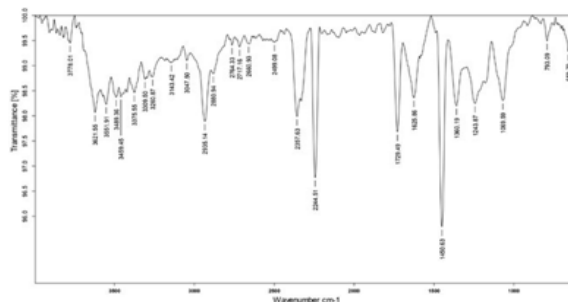


Figure 15. FTIR of M4 membrane

Iron oxide nanoparticles caused a fluctuation within the range of 3000-3500  $\text{cm}^{-1}$  (Figs. 13, 14 & 15) indicating N-H stretching and O-H stretching due to an increase in iron-oxide nanoparticles [7 & 8].

#### 4.3 Morphology studies by SEM

##### 4.3.1 HPA50 membrane (M1)

The surface morphology of the M1 membrane seen at a magnification of 20  $\mu\text{m}$  exhibited a smooth surface where the polyamide layer including piperazine, TMC, and PVA are randomly arranged on the surface of the PES substrate (Fig. 16(a)). The cross-sectional morphologies of the M1 membrane showed the



penetration of the PES substrate into polyester fabric support at a magnification of 200  $\mu\text{m}$  (Fig. 16(b)).

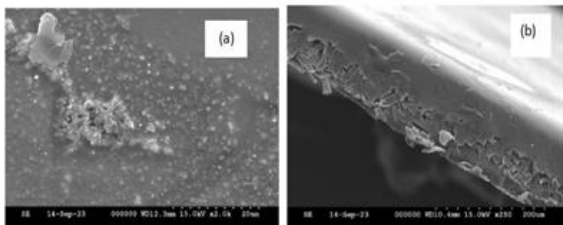


Figure 16. SEM images of M1 membrane

#### 4.3.2 PAN- $\text{Fe}_2\text{O}_3$ membranes (M2, M3 & M4)

PAN blended with varying percentages of iron oxide composite membranes resulted in consistent findings across different concentrations. At 0.005%, 0.01%, and 0.1%, uniform attachment of iron nanoparticles on the surface was observed at 50  $\mu\text{m}$  magnification (Figs. 17(a), 18(a), & 19 (a)). Cross-sectional images of membranes at higher magnifications of 500  $\mu\text{m}$  for 0.005% and 200  $\mu\text{m}$  for 0.01% and 0.1% displayed a thin layer of nanoparticles covering the PAN substrate (Figs. 17(b), 18(b), & 19 (b)).

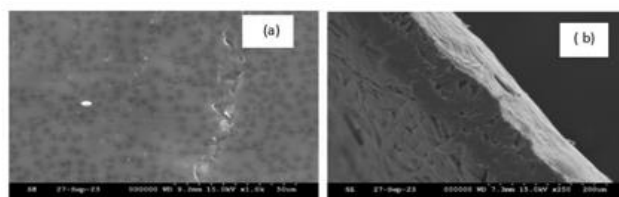


Figure 17. SEM images of M2 membrane

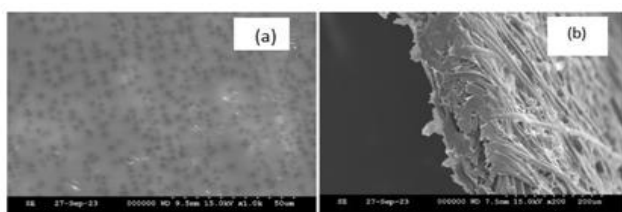


Figure 18. SEM images of M3 membrane

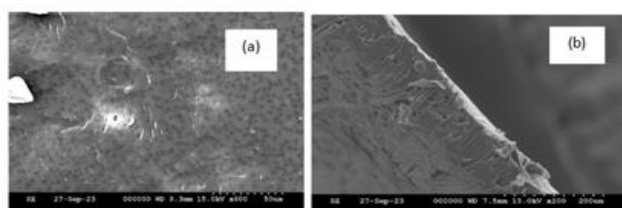


Figure 19. SEM images of M4 membrane

The average diameter of the iron oxide nanoparticles is

found to be 10.51 nm calculated by Image-J software (Fig. 17, 18, & 19).

#### 4.4 Membrane performance tests

The pure water flux of the M1 membrane increased with an increase in operating pressure. This observation suggests a direct relationship between pure water flux and operating pressure for the M1 membrane. An increase in operating pressure leads to higher driving forces across the membrane, resulting in enhanced water permeation through the membrane's porous structure. The pure water flux of membranes M2, M3, and M4 linearly increased with increase in iron nanoparticle concentration (Figs. 20, 21, & 22).

The presence of iron nanoparticles in the membrane matrix has a positive effect on water permeability, leading to a higher pure water flux [9]. The flux is constant at low gauge pressure for all membranes, hence '0 bar' is appropriate for time vs. flux studies.

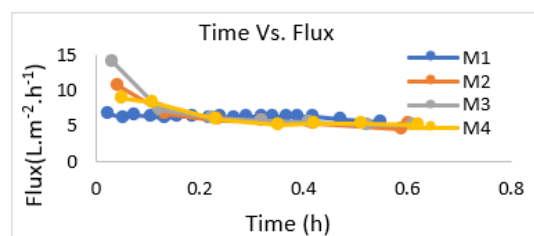


Figure 20. Pure water flux at '0 bar' pressure (Feed: Distilled water)

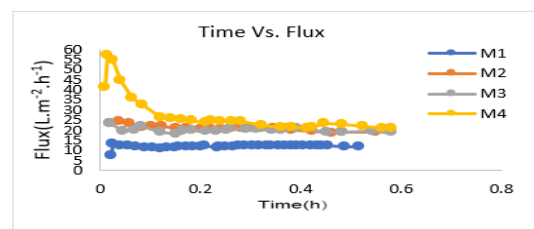


Figure 21. Pure water flux at '1 bar' pressure (Feed: Distilled water)

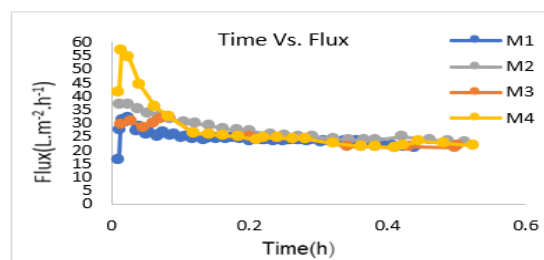


Figure 22. Pure water flux at '2 bar' pressure (Feed: Distilled water)



#### 4.5 Separation performance tests

##### 4.5.1 HPA50 membrane

Time vs. Flux graph of the HPA50 membrane (M1) with LiCl feed (0.06 wt%) solution showed an average fluxes of M1 is  $9.06 \text{ L.m}^{-2}.\text{h}^{-1}$ ,  $5.67 \text{ L.m}^{-2}.\text{h}^{-1}$ , and  $10.23 \text{ L.m}^{-2}.\text{h}^{-1}$  at pressures of 0.5 bar, 1 bar, and 2 bar respectively over a time period of 1.2 h (Fig. 23). The rejection rates of M1 membrane were 40%, 85%, and 83.9%. Highest rejection of  $\text{Li}^+$  ions is observed at 1 bar pressure (Fig.28).

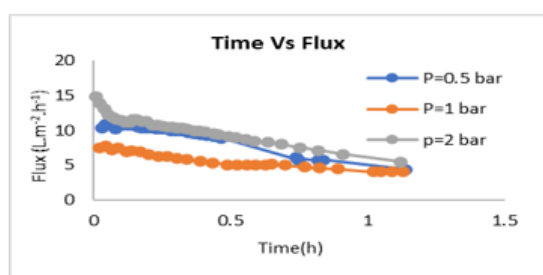


**Figure 23** Time vs. flux of M1 without SDS surfactant (Feed: 0.06 wt% of LiCl solution)

The rejection of M1 membrane with feed  $\text{MgCl}_2$  & LiCl (mass ratio = 2.4) showed an average flux of  $3.53 \text{ L.m}^{-2}.\text{h}^{-1}$ , and the rejection is 50% at 1 bar pressure (Fig. 24).

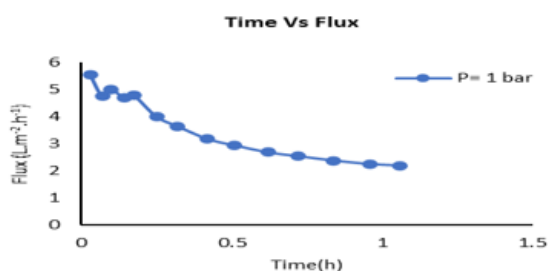


**Figure 24** Time vs. Flux for M1: feed LiCl+ $\text{MgCl}_2$  (mass ratio of  $\text{Mg}^{+2}/\text{Li}^+=2.4$ )

SDS is an anionic surfactant that helps to bind the lithium ions. In MEUF technique time vs. flux for the HPA50 membrane with feed LiCl solution and SDS showed an average fluxes of  $5.065 \text{ L.m}^{-2}.\text{h}^{-1}$ ,  $10.4469 \text{ L.m}^{-2}.\text{h}^{-1}$ ,  $10.0326 \text{ L.m}^{-2}.\text{h}^{-1}$  at operating pressures of 0.5 bar, 1 bar, and 2 bar respectively over a period of 0.7 h (Fig. 25). The rejection rates of M1 membrane by the addition of surfactant were 89.1%, 93%, 87% respectively.

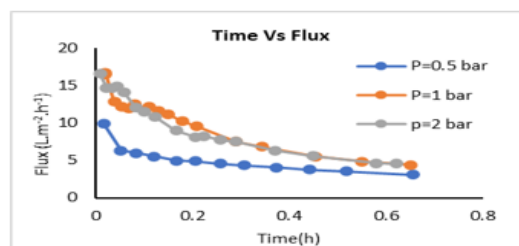


**Figure 25** Time vs. flux of M1 with SDS surfactant (Feed: 0.06 wt% of LiCl; 0.3 wt% of SDS)

For M1 membrane with mixed aqueous solution of LiCl &  $\text{MgCl}_2$  (mass ratio = 2.4), with SDS surfactant showed an average flux of  $1.246 \text{ L.m}^{-2}.\text{h}^{-1}$ , and the membrane rejected 70.2% of lithium ions (Fig. 26).

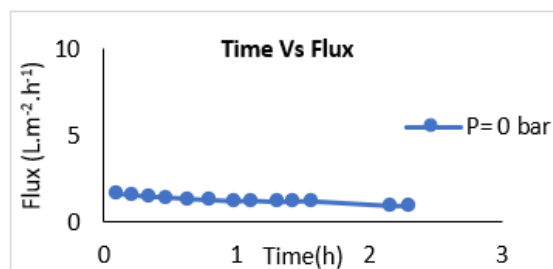


**Figure 26** Time vs. Flux for M1: feed LiCl+ $\text{MgCl}_2$  (mass ratio of  $\text{Mg}^{+2}/\text{Li}^+=2.4$ ; 0.3 wt% of SDS)

##### 4.5.2 PAN- $\text{Fe}_2\text{O}_3$ membranes

PAN membrane blended with iron nanoparticles with LiCl (0.06 wt%) feed solution at pressure 0.5 bar with different concentrations of iron nanoparticles M2 (0.005 wt%), M3 (0.01 wt%) and M4 (0.1 wt%). Flux is almost similar in all three membranes and there is no difference with increasing the iron nanoparticles concentration. The average flux of the membranes is  $9.37 \text{ L.m}^{-2}.\text{h}^{-1}$ ,  $9.84 \text{ L.m}^{-2}.\text{h}^{-1}$ , and  $9.75 \text{ L.m}^{-2}.\text{h}^{-1}$  at 0.5 bar pressure (Fig. 27). The time vs. flux experiments showed no rejection of lithium ions.

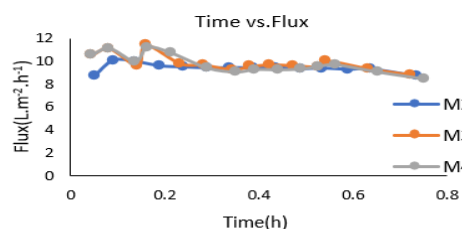


**Figure 27** Time vs. flux for M2, M3 and M4 membranes (Feed: 0.06 wt% of LiCl solution)



#### 4.6 Analytical studies

Feed, reject, and permeate samples of all the experiments were analysed for pH, conductivity, and TDS (Table 4).

**Table 4.3** Analytical results of samples for HPA50 membrane at different pressures.

S. No.	Feed Solution	Sample	Volume (ml)	pH	Conductivity (m.S/cm)	TDS (mg/L) C	Pressure (bar)	Rejection (R)=(Cf - Cp)/ Cf *100
1	LiCl=0.06 % (600 ppm)	Feed (f)	2000	6.48	0.95	610	0	40%
		Permeate (p)	1500	6.65	0.63	366		
		Reject (r)	300	7.3	2.68	1630		
2	LiCl=0.06 % (600 ppm)	Feed (f)	2000	6.53	0.91	395	1	83%
		Permeate (p)	1600	6.47	0.18	84		
		Reject (r)	250	5.8	2.02	1964		
3	LiCl=0.06 % (600 ppm)	Feed (f)	2000	6.64	0.83	574	2	83.9%
		Permeate (p)	1600	7.2	0.22	92		
		Reject (r)	250	6.2	3.13	2315		
4	Mg <sup>2+</sup> /Li <sup>+</sup> =2.4 (240 ppm)	Feed (f)	900	5.35	0.35	241	1	50.3%
		Permeate (p)	750	5.43	0.21	114		
		Reject (r)	150	6.5	0.58	520		
5	LiCl=0.06 % + SDS=0.3 % (600 ppm)	Feed (f)	1000	6.35	1.03	600	0.5	89.4%
		Permeate (p)	650	6.03	0.21	66		
		Reject (r)	350	6.11	1.9	1192		
6	LiCl=0.06 % + SDS=0.3 % (600 ppm)	Feed (f)	1000	6.03	0.92	600	1	93%
		Permeate (p)	660	6.58	0.12	42		
		Reject (r)	220	6.75	1.9	1260		
7	LiCl=0.06 % + SDS=0.3 % (600 ppm)	Feed (f)	1000	6.35	1.03	606	2	87.1%
		Permeate (p)	750	6.8	0.18	78		
		Reject (r)	250	6.4	2.83	1809		
8	Mg <sup>2+</sup> /Li <sup>+</sup> =2.4 + SDS=0.3 % (250 ppm)	Feed (f)	1000	6.2	0.39	255	0	70.2%
		Permeate (p)	750	6.53	0.16	76		
		Reject (r)	250	6.23	0.64	440		

#### 4.7 Effect of pressure vs. Li<sup>+</sup> recovery

Pressure directly affected the rejection capabilities of nanofiltration (NF) membranes [10], with low pressures between 0.5 to 2 bar showing significant removal rates of lithium ions. Addition of SDS surfactant at 0.3 wt% concentration, especially at lower pressures, improved removal efficiencies, resulting in removal percentages of 89.40%, 93%, and 83.90% for lithium ions (Fig. 28). The use of surfactants demonstrated a significant enhancement in separation efficiency, offering insights for optimizing membrane processes.

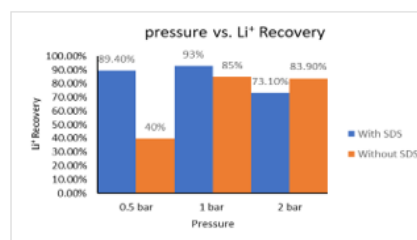


**Figure 28.** Pressure vs. Li<sup>+</sup> Recovery for HPA50 membrane (M1)

#### 4.8 Lithium ion detection by ICPMS

ICP-MS analysis of the HPA50 membrane with a feed LiCl solution at '0 bar' without any surfactants identified the area of peak for lithium ions. The size of the peak is directly related to the concentration of ions in the sample. Specifically, the peak area (Figs. 29, 30, & 31) for lithium ions in the retentate sample is greater at 0.1704 ( $\frac{\mu S-min}{cm}$ ) compared to the feed sample 0.0662 ( $\frac{\mu S-min}{cm}$ ) and permeate sample 0.0404 ( $\frac{\mu S-min}{cm}$ ). Similarly, ICP-MS analysis of two more studies conducted with different feed solutions (Table 5) indicated the addition of surfactant to the feed solution resulted in greater separation of lithium ions.

**Table 5.** ICP-MS analysis for the samples

S. No.	Feed Solution	Sample	Area of peak of lithium ( $\frac{\mu S-min}{cm}$ )	Rejection %
1	LiCl=0.06 % (600 ppm)	Feed (f)	0.0662	40
		Permeate (p)	0.0404	
		Reject (r)	0.1704	
2	LiCl=0.06 % + SDS=0.3 % (600 ppm)	Feed (f)	0.00582	93
		Permeate (p)	0.0066	
		Reject (r)	0.2076	
3	Mg <sup>2+</sup> /Li <sup>+</sup> =2.4 (240 ppm)	Feed (f)	0.0818	53
		Permeate (p)	0.0577	
		Reject (r)	0.1816	

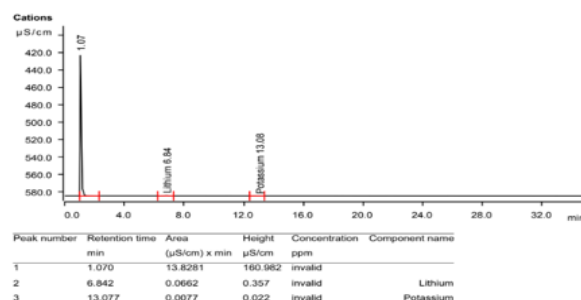


**Figure 29.** ICP-MS analysis of feed sample (LiCl feed)

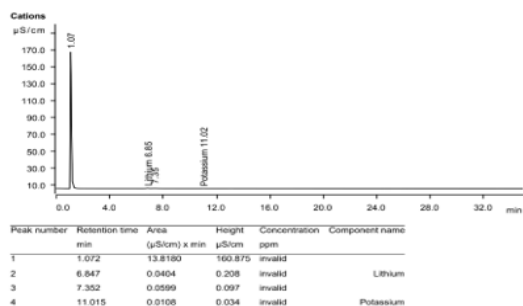


Figure 30. ICP-MS analysis of permeate sample (LiCl feed)

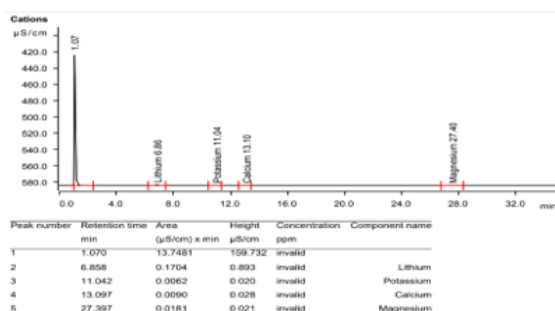


Figure 31. ICP-MS analysis of feed sample (LiCl feed)

## 5. Conclusions

- Membrane performance studies showed a consistent flux across different membranes (M1, M2, M3 & M4) under '0 bar' pressure, making it suitable for separation studies.
- The HPA50 membrane exhibited sharp crystalline peaks at 20°, 23°, and 25° in XRD analysis, while FTIR analysis identified functional groups such as amines, alkynes, methyl, sulfone, and vinyl groups. SEM analysis revealed a smooth surface representing the presence of piperazine, TMC, and PVC. Separation of lithium ions of the membrane showed rejection rates of 40%, 85%, and 83.9% at operating pressures of 0 bar, 1 bar, and 2 bar, respectively, with a LiCl aqueous feed solution. Addition of SDS surfactant increased rejection rates to 89.40%, 93%, and 83.90%, indicating a 49% increase in lithium ion rejection.
- PAN membranes blended with different concentrations of iron nanoparticles (0.005%, 0.01%, and 0.1%) were prepared for lithium-ion separation. XRD analysis exhibited sharp crystalline peaks at 18°, 23°, and 26°, indicating the presence of PAN and iron nanoparticles. FTIR analysis identified nitriles and methyl groups for PAN and iron nano particles. SEM analysis confirmed a

uniform and stable attachment of iron nanoparticles on the membrane surface. However, due to large pore sizes, no rejection of lithium ions was observed.

- In the ICP-MS analysis, the peak area of lithium ions in the reject sample is greater than the feed and permeate samples for all three different feed solutions, indicating the concentration of lithium ions in the reject sample. The addition of surfactant to the feed rejects more lithium ions, which is evident from the increased peak area of lithium ions of the reject sample.

## Acknowledgement

Authors acknowledge CSIR-Indian Institute of Chemical Technology, Tarnaka, Hyderabad, Telangana State, for facilitating conduction of experiments in Membrane Separation Laboratory at their CE & PT Division.

## References

- Li X, Mo Y, Qing W, Shao S, Tang CY, Li J. Membrane-based technologies for lithium recovery from water lithium resources: A review. *Journal of Membrane Science*. 2019 Dec 1;591:117317.
- Rivas, Bernabe L., Eduardo D. Pereira, and Ignacio Moreno-Villoslada. "Water-soluble polymer-metal ion interactions." *Progress in Polymer Science* 28.2 (2003): 173-208.
- Samper, Enrique, et al. "Removal of metal ions at low concentration by micellar-enhanced ultrafiltration (MEUF) using sodium dodecyl sulfate (SDS) and linear alkyl benzene sulfonate (LAS)." *Separation and purification technology* 65.3 (2009): 337-342.
- Oyarce, Estefania, et al. "Removal of lithium ions from aqueous solutions by an ultrafiltration membrane coupled to soluble functional polymer." *Separation and Purification Technology* 288 (2022): 120715.
- Xu, Ping, et al. "Positive charged PEI-TMC composite nanofiltration membrane for separation of Li<sup>+</sup> and Mg<sup>2+</sup> from brine with high Mg<sup>2+</sup>/Li<sup>+</sup> ratio." *Desalination* 449 (2019): 57-68.
- Xu, Ping, et al. "Positive charged PEI-TMC composite nanofiltration membrane for separation of Li<sup>+</sup> and Mg<sup>2+</sup> from brine with high Mg<sup>2+</sup>/Li<sup>+</sup> ratio." *Desalination* 449 (2019): 57-68.
- Fuguet, Elisabet, et al. "Critical micelle



concentration of surfactants in aqueous buffered and unbuffered systems." *Analytica Chimica Acta* 548.1-2 (2005): 95-100.

8. Jauhari, Jaidan, et al. "Synthesis and characteristics of polyacrylonitrile (PAN) nanofiber membrane using electrospinning method." *J. Chem. Technol. Metall* 56.4 (2021): 698-703.
9. Patel, Shabna, and Garudadhvaj Hota. "Iron oxide nanoparticle-immobilized PAN nanofibers: synthesis and adsorption studies." *RSC advances* 6.19 (2016): 15402-15414
10. Roobavannan, Sharaniya. *Enhancing the performance of lithium recovery in seawater with membrane distillation and manganese oxide metal-organic framework nanoparticles*. Diss. University of Technology Sydney (Australia), 2021.
11. Sun, Shu-Ying, et al. "Separation of magnesium and lithium from brine using a Desal nanofiltration membrane." *Journal of Water Process Engineering* 7 (2015): 210-217.
12. Wang, Li, et al. "Novel positively charged metal-coordinated nanofiltration membrane for lithium recovery." *ACS Applied Materials & Interfaces* 13.14 (2021): 16906-16915.
13. Sekhar, Sugali Chandra, et al. "Comprehensive treatment of aroma chemicals industrial effluent with substantial COD content by a novel PVP/polyamide composite hydrophilized RO membrane." *Chemical Engineering Journal* 468 (2023): 143658.